

Renormalization of effective interactions in a negative charge-transfer insulator

Priyanka Seth,^{1,2} Oleg E. Peil,^{1,3,4} Leonid Pourovskii,^{1,4} Markus Betzinger,⁵ Christoph Friedrich,⁵ Olivier Parcollet,² Silke Biermann,¹ Ferdi Aryasetiawan,⁶ and Antoine Georges^{1,3,4}

¹*Centre de Physique Théorique, École Polytechnique, CNRS, Université Paris-Saclay, 91128 Palaiseau, France*

²*Institut de Physique Théorique (IPhT), CEA, CNRS, 91191 Gif-sur-Yvette, France*

³*Department of Quantum Matter Physics, University of Geneva,*

24 Quai Ernest-Ansermet, 1211 Geneva 4, Switzerland

⁴*Collège de France, 11 place Marcelin Berthelot, 75005 Paris, France*

⁵*Peter Grünberg Institut and Institute for Advanced Simulation, Forschungszentrum Jülich and JARA, 52425 Jülich, Germany*

⁶*Department of Physics, Division of Mathematical Physics, Professorsgatan 1, 223 62 Lund, Sweden*

(Dated: September 10, 2018)

We compute from first principles the effective interaction parameters appropriate for a low-energy description of the rare-earth nickelate LuNiO_3 involving the partially occupied e_g states only. The calculation uses the constrained random-phase approximation and reveals that the effective on-site Coulomb repulsion is strongly reduced by screening effects involving the oxygen- p and nickel- t_{2g} states. The long-range component of the effective low-energy interaction is also found to be sizeable. As a result, the effective on-site interaction between parallel-spin electrons is reduced down to a small negative value. This validates effective low-energy theories of these materials proposed earlier. Electronic structure methods combined with dynamical mean-field theory are used to construct and solve an appropriate low-energy model and explore its phase diagram as a function of the on-site repulsion and Hund's coupling. For the calculated values of these effective interactions we find, in agreement with experiments, that LuNiO_3 is a metal without disproportionation of the e_g occupancy when considered in its orthorhombic structure, while the monoclinic phase is a disproportionated insulator.

I. INTRODUCTION

The interplay between the atomic physics and strong covalent bonding in transition-metal oxides (TMO) results in a variety of fascinating phenomena¹. The energy scale spanned by the hybridized states formed by the d orbitals of the transition metal and the p states of oxygen is typically of order 10 eV. However, it is often useful for physical understanding to use a “low-energy” description in which only a subset of the metal-oxygen antibonding states is retained, namely the partially occupied states in proximity to the Fermi level. Those usually span a narrower energy window of a few electron-Volts. Going over from the full high-energy description to a low-energy model allows one to reduce the dimension of the Hilbert space considerably, and quite often provides physical insight into the behavior of a material. This is particularly relevant to late transition-metal oxides involving antibonding e_g orbitals, as exemplified by the Zhang-Rice single-band picture of cuprates².

A price to pay for this simplification is the renormalization of interaction parameters when high energy states are integrated out. These renormalizations can be large, and evaluating the proper values of low-energy interactions is a challenging problem of great practical importance. In all TMOs, an important interaction is the Coulomb repulsion U_{dd} between localized, atomic-like, d states of the TM cation. In late TMOs, however, the energy scale relevant for low-energy states is the charge-transfer energy, which can be much smaller³ than U_{dd} .

A class of materials in which this issue is particularly relevant is the family of rare-earth nickelates, RNiO_3 . These materials have a very large degree of covalency between the Ni and O states⁴. This may result in the charge-transfer en-

ergy being very small in magnitude and possibly negative^{5–9}, leading to the appearance of holes on ligand (oxygen) states in the ground-state¹⁰. A direct confirmation of the presence of ligand holes has been recently provided by X-ray absorption and resonant inelastic X-ray scattering experiments¹¹.

The metal-insulator transition (MIT) of the RNiO_3 series is accompanied by a structural transition from the high- T orthorhombic structure to a low- T monoclinic structure. In the latter, the uniform octahedra of the orthorhombic structure distort into a set of compressed octahedra with short Ni-O bonds (SB) and a set of expanded octahedra with long bonds (LB). A qualitative, somewhat extreme, picture of the low- T phase^{8,12} is to assign the configuration d^8 to the Ni sites of the LB octahedra and $d^8\bar{L}^2$ (with two ligand holes delocalized on neighboring oxygens) to the SB octahedra. This is in contrast to the nominal valence Ni- d^7 suggested by a naive counting in the ionic limit (with R^{3+} , O^{2-}) so that the picture above can be summarized as $d^7 + d^7 \rightarrow d^8 + d^8\bar{L}^2$. Correspondingly, in this extreme picture, the LB sites would carry a spin-1 magnetic moment, while the SB sites would carry no magnetic moment (the Ni-moment being screened by the oxygen holes¹²). Note that this disproportionation does not necessarily correspond to a large amplitude charge ordering since each oxygen actually belongs to both a SB and LB octahedron so that the average charge on each octahedron can remain weakly modulated or even uniform.

Subedi *et al.*¹³ recently proposed a low-energy description of the electronic structure of the RNiO_3 series, involving only the p - d hybridized antibonding states with e_g symmetry close to the Fermi level. In this description, the above disproportionation can be viewed as $e_g^1 + e_g^1 \rightarrow e_g^2 + e_g^0$ (Fig. 1). Building on earlier ideas by Mazin *et al.*¹⁴, these authors showed that such a disproportionation is favored by a strong reduc-

tion of the effective U acting on the low-energy e_g states and by a large value of the low-energy Hund's coupling J . More precisely, the monoclinic distortion splits the low-energy e_g states into two groups of states separated by a Peierls-like energy gap Δ_s (note that this gap opens at the energy corresponding to half-filling, and is hence not directly responsible for the transition into the insulating state of these nominally quarter-filled compounds). Using dynamical mean-field theory (DMFT)¹⁵ in combination with density-functional calculations, a U - J phase diagram was established for the low-energy model, demonstrating that a disproportionated insulating phase is present in the range of coupling parameters where the parallel-spin interaction $U^{\sigma\sigma} = U - 3J$ is smaller than the Peierls gap Δ_s .

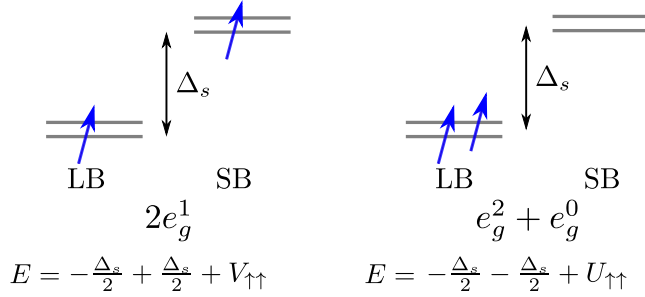


FIG. 1. Schematic picture of the disproportionation associated with the metal-insulator transition for a two-site model consisting of a LB site and a SB site. The energy of the LB site is lowered as compared to that of the SB site by the Peierls energy Δ_s . Each site carries two e_g orbitals. In the doubly occupied configuration, each orbital is occupied by a single electron with parallel spins, in accordance with Hund's rules. An on-site interaction $U^{\sigma\sigma}$ between electrons with parallel spins is considered, as well as an inter-site interaction $V^{\sigma\sigma}$. In the atomic limit where hopping is neglected, the criterion for stabilizing the disproportionated state $e_g^2 + e_g^0$ over the uniform one $e_g^1 + e_g^1$ reads: $U^{\sigma\sigma} - V^{\sigma\sigma} < \Delta_s$. The extension of this criterion to a whole lattice in the presence of hopping is discussed in the main text.

The low-energy picture of Subedi *et al.*¹³ is in good agreement both with experiments (e.g. optical spectroscopy^{16,17}) and with earlier DMFT calculations including all Ni- d and O- p states¹². However, the question of whether the strongly renormalized value of the effective low-energy interaction $U^{\sigma\sigma} = U - 3J$ is indeed realistic remains widely open. A first-principles calculation of these low-energy effective interactions is obviously highly desirable. Furthermore, Ref.13 did not consider the role of inter-site interactions, which are surely induced when downfolding onto a low-energy model and are known to be important in materials with electronic disproportionation or charge ordering. When the intersite interaction V between the LB and SB sites is included, the more accurate condition for charge disproportionation becomes $U_{\sigma\sigma} - V_{\sigma\sigma} < \Delta_s$ for the two-site case treated in the atomic limit, as depicted in Fig. 1. For the full problem one needs to include hopping, correctly treat the lattice connectivity, and also include the effect of long-range Coulomb interactions, which are important in insulators. There is little experimental spectroscopic in-

formation on such long-range interactions. The aim of the present article is to attempt a first-principles determination of the appropriate low-energy parameters, and examine the physical consequences of the obtained values in light of the issues discussed above.

The approach that we shall adopt is the constrained random-phase approximation (cRPA)¹⁸. This method has proven successful in calculating interaction parameters between electrons in localized d or f states assumed to be screened by more extended s and p states^{19–25}. In this paper, we apply this method to calculate the interaction parameters corresponding to low-energy states of LuNiO₃, which exhibits the largest distortion amongst the family of RNiO₃. It is worth emphasizing that such a system represents a true challenge to cRPA because the contributions to screening come both from extended O- p , with possible ligand holes, which are very close in energy to the e_g states and strongly hybridized, and also from localized completely filled t_{2g} states of the Ni ions.

In this paper we show that, despite these challenges, the cRPA method is indeed able to produce the large renormalization of the Coulomb repulsion U . We also show that $U_{\sigma\sigma}$ is further effectively reduced due to intersite Coulomb interactions down to values comparable to the Peierls gap Δ_s , hence establishing on firm grounds the low-energy description suggested previously^{13,14}, with the additional twist of large non-local interactions effectively renormalizing the local ones. We calculate the phase diagram of LuNiO₃ within a combination of density-functional theory-based electronic structure and dynamical mean-field theory (DFT+DMFT), including the intersite interactions at a static mean-field level. For the cRPA values of U , J and of the inter-site interactions, our DFT+DMFT calculations yield a metallic state for the orthorhombic phase and a disproportionated insulator for the monoclinic one, in agreement with experiments.

This article is organized as follows. In Sec. II, we provide an introduction to the electronic structure of LuNiO₃ and to the effective low-energy description in terms of e_g states. In Sec. III we implement the constrained random-phase approximation and compute the resulting *ab initio* interaction parameters. In Sec. IV, we summarize the *ab initio* construction of the low-energy effective model and explore its phase diagram within the DFT+DMFT framework for both the orthorhombic and monoclinic phases, as a function of U and J . We show that the cRPA-calculated values of these parameters correspond to a location of each of the two structures in this phase diagram which is physically consistent. Our results and findings are briefly summarized and discussed in Sec. V.

II. ELECTRONIC STRUCTURE AND LOW-ENERGY MODEL

The electronic structure of both the low-temperature monoclinic (space group $P2_1/n$, see Fig. 2) and high-temperature orthorhombic ($Pbnm$) phases of LuNiO₃ have been calculated using the experimental lattice structures provided in Ref. 26 (at $T = 673\text{K}$ for $Pbnm$ and $T = 533\text{K}$ for $P2_1/n$). The unit cells of both structures contain four formula units,

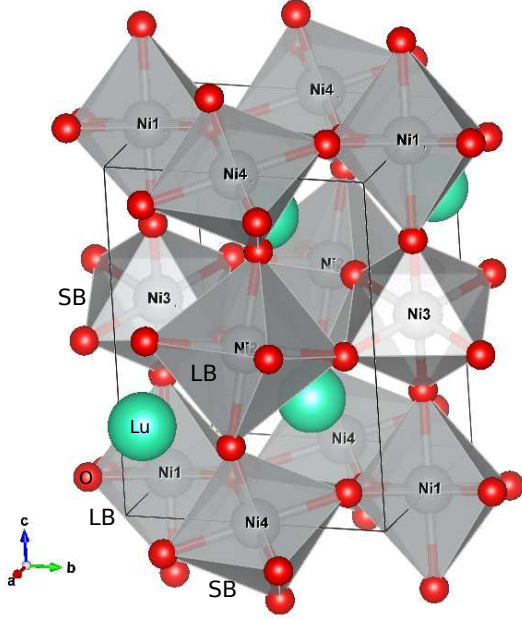


FIG. 2. LuNiO_3 in the monoclinic phase. Oxygen atoms (red) form distorted octahedra containing Ni (grey). This structure is intercalated with Lu atoms (turquoise). The short-bond (SB) and long-bond (LB) octahedra are identified. The labels of the Ni atoms correspond to the positions given in Table I.

but the monoclinic one differs by having two distinct types of NiO_6 octahedra, one with short Ni-O bonds and one with long bonds corresponding to compressed and expanded octahedra. For the reader's convenience we list the fractional coordinates of the Ni sites in the monoclinic cell in Table I.

TABLE I. Fractional coordinates and types of Ni sites in the monoclinic structure of LuNiO_3 . Ni_1 and Ni_2 are of the LB type and lie diagonally across from each other, as do the SB sites Ni_3 and Ni_4 . Ni_1 has as nearest neighbors $2 \times \text{Ni}_3$ in the z direction and $4 \times \text{Ni}_4$ in the x - y plane.

	type	X	Y	Z
Ni_1	LB	$\frac{1}{2}$	0	0
Ni_2	LB	0	$\frac{1}{2}$	$\frac{1}{2}$
Ni_3	SB	$\frac{1}{2}$	0	$\frac{1}{2}$
Ni_4	SB	0	$\frac{1}{2}$	0

In our density-functional-theory (DFT) calculations within the local-density approximation (LDA) we have employed the full-potential augmented-plane-wave (FP-LMTO) method as implemented in the FLEUR package^{27,28}. All calculations were performed using a k -mesh consisting of $4 \times 4 \times 2$ points.

The calculated low-energy band structure of monoclinic LuNiO_3 (Fig. 3) features a manifold of 8 e_g bands in the range of $[-0.4; 1.9]$ eV around the Fermi level, with the filled t_{2g} bands located below -0.7 eV in energy and, hence, well separated from the e_g ones. We note that a small ‘Peierls gap’ $\Delta_s^{\text{DFT}} \simeq 0.25$ eV separates the e_g bands into 2 sets of 4 bands (except an isolated point U), at an energy corresponding to

the nominal filling of two electrons per site (half-filling), i.e. about $+0.5$ eV above the LDA Fermi level. The Peierls gap originates from the existence of two types of sites in the distorted monoclinic phase: LB sites are pushed down in energy relative to the more covalent SB sites, for which the Ni d and O p orbitals overlap more. The DFT band structure of the orthorhombic phase is quite similar to that of the monoclinic phase (see e.g. Fig. 1 of Ref. 13), apart from the fact that the Peierls gap is of course closed in this case.

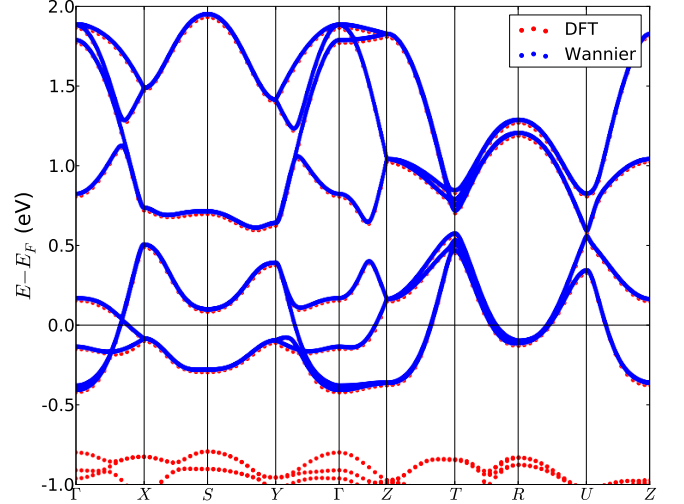


FIG. 3. The band structure of the monoclinic phase of LuNiO_3 for a unit cell consisting of four formula units. The DFT bands are shown in red and the band structure produced by the Wannier-basis low-energy Hamiltonian is shown in blue. Within the numerical accuracy, the Wannier bands are identical to the DFT e_g bands. The Peierls gap splits the set of 8 e_g bands into two separated sets of 4 bands.

In order to construct the quadratic part of the low-energy model, we downfold the states around the Fermi energy. A set of maximally localized Wannier functions representing correlated e_g states on Ni sites was constructed from the 8 e_g bands using the WANNIER90 package²⁹. Given the absence of entanglement between the e_g bands and the rest of the electronic structure in LuNiO_3 , the projection from the space of Kohn-Sham e_g eigenstates onto the Wannier basis is simply a unitary transformation. Hence, by diagonalizing the resulting low-energy Wannier Hamiltonian, one reproduces the original DFT bands, as shown in Fig. 3.

III. CONSTRAINED-RANDOM-PHASE APPROXIMATION

A. Method description

With the quadratic part of the low-energy Hamiltonian for the e_g states, we perform *ab initio* calculations of the corresponding interaction terms using the constrained random-phase approximation (cRPA)¹⁸.

The main idea behind the cRPA is to write the effective interactions suitable for a low-energy multi-band model as the

matrix elements of a partially screened interaction in the chosen localized basis. Calculations within the cRPA method start from the evaluation of the bare (unscreened) Coulomb vertex v . The partial polarization function $P_r(\omega)$ is then calculated. This describes the screening of v within RPA by including all particle-hole transitions except those within the low-energy e_g subspace, i.e., $P_r(\omega) = P(\omega) - P_{e_g}(\omega)$, where $P(\omega)$ is the total polarization function and $P_{e_g}(\omega)$ is the contribution of all transitions within the low-energy subspace. Processes within the low-energy subspace will be subsequently treated explicitly by solving the low-energy Hamiltonian with more sophisticated many-body techniques beyond the RPA, such as DMFT.

The partially screened frequency-dependent interaction is obtained as $W_r(\omega) = v/[1 - P_r(\omega)v]$. The Hubbard interactions are then obtained from matrix elements of the static limit $W_r(\omega = 0)$ of this effective interaction. An important advantage of the cRPA is its ability to easily treat intersite interactions, as demonstrated in Refs. 30–32.

The cRPA procedure is unambiguously defined when a subset of correlated states is separated from the rest of the bands, as it is the case with the e_g bands of LuNiO_3 . However, in the case of an entanglement between correlated and uncorrelated bands one faces the problem of determining which screened processes should be included in $P_r(\omega)$. The two schemes that have been proposed to date to handle this issue, disentanglement³³ and projection³⁴, both give identical results in our case with $P_{e_g}(\omega)$ including all transitions within the e_g manifold, as the 8 e_g bands are well separated from all other bands.

In our calculations, the on-site and inter-site effective interactions between Ni e_g states are obtained using the cRPA functionality of the SPEX code, a GW code based on the FLEUR²⁷ electronic structure package³⁵. 800 Kohn-Sham bands up to the energy cut-off of 140 eV were included in $P(\omega)$ and, correspondingly, $P_r(\omega)$. In order to describe correctly semicore and high-energy Kohn-Sham states we extended the FLAPW basis by including additional local orbitals^{36,37}. Namely, we included local orbitals for the 3s, 4s, 5s, 3p, 4p, 5p, 3d, 4d, 4f and 5f shells of Ni; 2s, 3s, 2p, 3p, 3d, 4d, 4f and 5f shells of O; 5s, 6s, 7s, 5p, 6p, 7p, 5d, 6d, 4f, and 5f shells of Lu, as well as 6g and 7h shells on all atoms.

B. cRPA Results for LuNiO_3

Here we discuss the interaction parameters for the low-energy models as obtained by cRPA. We consider only the density-density interaction terms for parallel and anti-parallel spins. Note that the coupling constants J_X and J_P , corresponding respectively to the spin-flip and pair-hopping terms can be obtained from the density-density terms under the assumption of rotational invariance. All results are given in the basis of the eight e_g orbitals, ordered as z^2 and $x^2 - y^2$ for each of the four Ni sites as given above. The results for the orthorhombic phase are given in Table II and those for the monoclinic phase in Table III.

1. Orthorhombic LuNiO_3

For the orthorhombic phase of LuNiO_3 , the average density-density interaction between electrons with opposite spins in the same orbital is found to be $U = 1.65$ eV, that between opposite spins in different orbitals is $U' = 0.99$ eV. The interaction between parallel spins in different orbitals is the smallest, in accordance with Hund's rule, being reduced to $U^{\sigma\sigma} = U' - J = 0.66$ eV. We observe that, despite the orthorhombic distortion, these parameters obey almost perfectly the relation $U' = U - 2J$ expected for a cubic system, with $U = 1.65$ eV, $J = 0.33$ eV.

The average nearest-neighbor parallel-spin interaction $V_1^{\sigma\sigma}$ is 0.42 eV, where the average is taken evenly over both neighbors in the unit cell, comparable to the average on-site parallel-spin interaction $U' - J = 0.66$ eV. Additionally, the next-nearest-neighbor parallel-spin interaction $V_2^{\sigma\sigma}$ can be estimated from e.g. Ni_1 and Ni_2 to be 0.30 eV.

2. Monoclinic LuNiO_3

For the monoclinic phase we obtain for the averaged parameters $U = 1.83$ eV, $U' = 1.09$ eV and $U' - J = 0.74$ eV, which is fairly consistent with the Kanamori parametrisation for a cubic system with $U = 1.83$, $J = 0.37$ eV's.

The on-site parallel-spin interaction $U^{\sigma\sigma} = U - 3J = 0.74$ eV is again of a similar order of magnitude to the average nearest-neighbor parallel-spin interaction $V_1^{\sigma\sigma} = 0.44$ eV. In this case, due to the distortions in the structure, the average needs to be weighted to account for the fact that Ni_1 has 4 Ni_4 atoms and 2 Ni_3 atoms as neighbors. For the next-nearest-neighbor interaction, we obtain $V_2^{\sigma\sigma} = 0.31$ eV.

3. Long-range nature of interactions

For both phases, we notice that the nearest-neighbor intersite interactions V_1 , for example between Ni_1 and Ni_3 and between Ni_1 and Ni_4 , are found to be non-negligible. It must be emphasized that the contributions to screening from particle-hole transitions within the e_g manifold of bands are excluded in the cRPA procedure. Indeed, the effective interactions obtained from cRPA are to be used in the low-energy effective e_g model, and further screening relies on the many-body treatment of this model (e.g. with DMFT). As a result, the interactions in the low-energy effective model are screened exclusively by interband transitions, as in an insulator, and thus one should expect significant long-range Coulomb interactions. Indeed, the second nearest-neighbor interactions V_2 are likewise quite large. Upon closer inspection, it is clear that the interactions up to the second shell of neighbors decay as $1/R$, indicating that long-range interactions must be accounted for to reach an accurate description of the physics of these materials. The situation is comparable to the recently studied case of $\text{Sn/Si}(111)$ ^{30–32}: there it was shown that the continuum limit that allows to parametrize the interaction tail as $\frac{V_1}{R}$ with the nearest neighbor interaction $V_1 = \epsilon^{-1}V_1^{\text{bare}}$, with ϵ the

TABLE II. $U_{mm'}$ for anti-parallel and parallel spins for orthorhombic LuNiO_3 . All values in eV. Two-index parameters are related to four-index ones as $U_{mm'}^{\sigma\sigma} = U_{mm'mm'}$, $U_{mm'}^{\sigma\sigma} = U_{mm'mm'} - U_{mm'm'm}$.

$U_{mm'}^{\sigma\sigma}$ (anti-parallel spin)							
Ni_1, z^2	$\text{Ni}_1, x^2 - y^2$	Ni_2, z^2	$\text{Ni}_2, x^2 - y^2$	Ni_3, z^2	$\text{Ni}_3, x^2 - y^2$	Ni_4, z^2	$\text{Ni}_4, x^2 - y^2$
1.77	0.99	0.32	0.30	0.62	0.43	0.39	0.42
0.99	1.54	0.30	0.27	0.43	0.33	0.40	0.45
0.32	0.30	1.77	0.99	0.39	0.40	0.62	0.43
0.30	0.27	0.99	1.54	0.42	0.45	0.43	0.33
0.62	0.43	0.39	0.42	1.77	0.99	0.32	0.30
0.43	0.33	0.40	0.45	0.99	1.54	0.30	0.27
0.39	0.40	0.62	0.43	0.32	0.30	1.77	0.99
0.42	0.45	0.43	0.33	0.30	0.27	0.99	1.54

$U_{mm'}^{\sigma\sigma}$ (parallel spin)							
Ni_1, z^2	$\text{Ni}_1, x^2 - y^2$	Ni_2, z^2	$\text{Ni}_2, x^2 - y^2$	Ni_3, z^2	$\text{Ni}_3, x^2 - y^2$	Ni_4, z^2	$\text{Ni}_4, x^2 - y^2$
0.00	0.66	0.32	0.30	0.59	0.42	0.38	0.41
0.66	0.00	0.30	0.27	0.42	0.33	0.39	0.42
0.32	0.30	0.00	0.66	0.38	0.39	0.59	0.42
0.30	0.27	0.66	0.00	0.41	0.42	0.42	0.33
0.59	0.42	0.38	0.41	0.00	0.66	0.32	0.30
0.42	0.33	0.39	0.42	0.66	0.00	0.30	0.27
0.38	0.39	0.59	0.42	0.32	0.30	0.00	0.66
0.41	0.42	0.42	0.33	0.30	0.27	0.66	0.00

TABLE III. $U_{mm'}$ for anti-parallel and parallel spins for monoclinic LuNiO_3 . All values in eV. Two-index parameters are related to four-index ones as $U_{mm'}^{\sigma\sigma} = U_{mm'mm'}$, $U_{mm'}^{\sigma\sigma} = U_{mm'mm'} - U_{mm'm'm}$.

$U_{mm'}^{\sigma\sigma}$ (anti-parallel spin)							
Ni_1, z^2	$\text{Ni}_1, x^2 - y^2$	Ni_2, z^2	$\text{Ni}_2, x^2 - y^2$	Ni_3, z^2	$\text{Ni}_3, x^2 - y^2$	Ni_4, z^2	$\text{Ni}_4, x^2 - y^2$
1.73	1.07	0.32	0.31	0.63	0.46	0.39	0.44
1.07	1.88	0.31	0.29	0.45	0.37	0.43	0.50
0.32	0.31	1.73	1.07	0.39	0.42	0.63	0.46
0.31	0.29	1.07	1.88	0.44	0.50	0.45	0.37
0.63	0.45	0.39	0.44	1.82	1.12	0.32	0.31
0.46	0.37	0.42	0.50	1.12	1.89	0.31	0.29
0.39	0.43	0.63	0.45	0.32	0.31	1.82	1.12
0.44	0.50	0.46	0.37	0.31	0.29	1.12	1.89

$U_{mm'}^{\sigma\sigma}$ (parallel spin)							
Ni_1, z^2	$\text{Ni}_1, x^2 - y^2$	Ni_2, z^2	$\text{Ni}_2, x^2 - y^2$	Ni_3, z^2	$\text{Ni}_3, x^2 - y^2$	Ni_4, z^2	$\text{Ni}_4, x^2 - y^2$
0.00	0.74	0.32	0.31	0.60	0.45	0.38	0.43
0.74	0.00	0.31	0.29	0.45	0.37	0.42	0.48
0.32	0.31	0.00	0.74	0.38	0.42	0.60	0.45
0.31	0.29	0.74	0.00	0.43	0.48	0.45	0.37
0.60	0.45	0.38	0.43	0.00	0.83	0.32	0.31
0.45	0.37	0.42	0.48	0.83	0.00	0.31	0.29
0.38	0.42	0.60	0.45	0.32	0.31	0.00	0.82
0.43	0.48	0.45	0.37	0.31	0.29	0.82	0.00

macroscopic dielectric constant, is already reached at nearest neighbor distances. Similarly, in graphene, the long-range tail of the interactions was argued to be responsible for the necessary screening to prevent the system from becoming a Mott insulator³⁸. More generally, the effects of non-local interactions in correlated materials and models thereof have recently raised tremendous interest in the community^{39–49}, within different lattice geometries.

From Tables II and III one may also conclude that the spin dependence of intersite interactions is negligible; the exchange interaction arises due to direct overlap of the e_g or-

bitals and, therefore, is well localized. Hence, from now on we will suppress the spin subscripts in the intersite interactions V .

IV. PHYSICAL CONSEQUENCES FOR LuNiO₃ AND DMFT CALCULATIONS

A. Effective theory for low-energy e_g states

From the sections above, we can infer the following effective Hamiltonian for a description of LuNiO₃ involving only low-energy e_g states:

$$\hat{H} = \hat{H}_0 + \sum_i \hat{H}_U^{(i)} + \hat{H}_V. \quad (1)$$

In this expression, \hat{H}_0 is the single-electron part of the effective Hamiltonian. Within the DFT+DMFT framework, \hat{H}_0 is constructed as:

$$\hat{H}_0 = \hat{H}_{\text{DFT}}^0 - \hat{H}_{dc}, \quad (2)$$

with \hat{H}_{DFT}^0 the single-electron Kohn-Sham Hamiltonian for e_g bands, as obtained from DFT(-LDA) and \hat{H}_{dc} is a double-counting correction to be detailed below. The many-body terms \hat{H}_U and \hat{H}_V are local (on-site) and inter-site interaction terms, respectively. For the local term, the full Kanamori Hamiltonian appropriate for e_g states is considered, namely on each lattice site (i):

$$\begin{aligned} \hat{H}_U = & U \sum_m \hat{n}_{m\uparrow} \hat{n}_{m\downarrow} + (U - 2J) \sum_{m \neq m'} \hat{n}_{m\uparrow} \hat{n}_{m'\downarrow} \\ & + (U - 3J) \sum_{m < m', \sigma} \hat{n}_{m\sigma} \hat{n}_{m'\sigma} \\ & - J \sum_{m \neq m'} c_{m\uparrow}^\dagger c_{m\downarrow} c_{m'\downarrow}^\dagger c_{m'\uparrow} + J \sum_{m \neq m'} c_{m\uparrow}^\dagger c_{m\downarrow}^\dagger c_{m'\downarrow} c_{m'\uparrow}. \end{aligned}$$

The inter-site term is taken to be of the form:

$$\hat{H}_V = \frac{1}{2} \sum_{i \neq j} V_{ij} \hat{n}_i \hat{n}_j.$$

In this expression, the coupling constants U , J and $V_{ij} = V_1/R_{ij}$ (with R_{ij} the distance between the two atomic sites i, j) are determined from the cRPA calculations presented above.

In the following, we show that this low-energy effective model with cRPA values of the interaction parameters provides a satisfactory description of the physics of LuNiO₃. This is done by using the DFT+DMFT framework in order to construct and solve the low-energy model. We find that intersite interactions must be taken into account in this low-energy description: they are included in our calculations at the level of Hartree mean-field theory. Finally, these findings are discussed in relation to the low-energy picture of rare-earth nickelates proposed in Ref. 13.

B. Hartree treatment of long-range interactions

In order to take the intersite terms into account we employ the Hartree approximation for long-range interactions. Note

that this is consistent with the DMFT approach, in which only local interactions have dynamical effects, while non-local interactions are treated at the static mean-field level. In the Hartree approximation, \hat{H}_V reduces to:

$$\hat{H}_V \rightarrow \frac{1}{2} \sum_{i \neq j} V_{ij} [n_i \hat{n}_j + n_j \hat{n}_i - n_i n_j],$$

with the effective Hartree one-body Hamiltonian and potential

$$\hat{H}_{\text{eff}} = \sum_i V_H(i) \hat{n}_i, \quad V_H(i) = \sum_{j \neq i} V_{ij} n_j.$$

The total energy from the interacting part of the Hamiltonian is thus

$$E_V[\{n_i\}] = \frac{1}{2} \sum_{i \neq j} V_{ij} n_i n_j = \frac{1}{2} \sum_i V_H(i) n_i. \quad (3)$$

Let us now consider the present case of the Ni sublattice in LuNiO₃. It can be well approximated by the NaCl-type bipartite lattice with two inequivalent, LB and SB, sublattices with occupancies n_{LB} and n_{SB} per site, respectively. Given that the system is charge neutral the formally diverging term on the r.h.s. of Eq. (3) can be summed using the Madelung method, resulting in the following sublattice potentials:

$$\begin{aligned} V_H(\text{LB}) &= -MV_1(n_{\text{LB}} - n_{\text{SB}})/2, \\ V_H(\text{SB}) &= +MV_1(n_{\text{LB}} - n_{\text{SB}})/2, \end{aligned}$$

where M is the Madelung constant for the NaCl lattice and the uniform part of the potential is dropped.

By comparing this result with the Hartree term with only nearest-neighbor interactions,

$$\begin{aligned} V_H^{nn}(\text{LB}) &= -z_{\text{eff}} V_1 (n_{\text{LB}} - n_{\text{SB}})/2, \\ V_H^{nn}(\text{SB}) &= +z_{\text{eff}} V_1 (n_{\text{LB}} - n_{\text{SB}})/2, \end{aligned}$$

we can identify M as an effective connectivity of the lattice

$$z_{\text{eff}} = M \approx 1.747.$$

Note that the effect of the Madelung summation is that the effective connectivity z_{eff} is significantly reduced as compared to the lattice connectivity $z = 6$.

The Hartree potential above can be viewed as a site-dependent contribution to the self-energy coming from the intersite interactions, which reads:

$$\Sigma_\alpha^V = z_{\text{eff}} V_1 (n_{\bar{\alpha}} - n_\alpha)/2. \quad (4)$$

In this expression, $\bar{\alpha}$ designates the opposite sublattice relative to α , i.e. if $\alpha = \text{SB}$ then $\bar{\alpha} = \text{LB}$ and vice versa; n_α is the e_g occupancy of the corresponding site.

C. Atomic limit

Before discussing the DFT+DMFT results, we first consider the atomic limit in which all hopping terms in the Hamiltonian (1) are set to zero so that \hat{H}_0 contains only an on-site

Peierls potential equal to $-\Delta_s/2$ on LB sites and $+\Delta_s/2$ on SB sites (see Fig. 1). We will compare in this limit the energies of two states: the uniform one (UN) $n_{LB} = n_{SB} = 1$ and the fully disproportionated one (FD) $n_{LB} = 2, n_{SB} = 0$.

The contribution of the on-site Peierls potential to the energy is $-\Delta_s \sum_{i \in LB} n_i/2 + \Delta_s \sum_{i \in SB} n_i/2$: it vanishes in the uniform state and provides an energy gain $-\Delta_s(N_s/2)$ in the FD state, with N_s the total number of lattice sites. The on-site interaction energy vanishes too in the UN state, and is equal to $+U^{\sigma\sigma}N_s/2$ in the FD state with $U^{\sigma\sigma} = U - 3J$, since two electrons on a LB site will occupy the high-spin Hund's rule configuration with one electron in each of the two e_g orbitals. Finally, using the above expressions in the Hartree approximation, the contribution of the inter-site interactions to the energy reads:

$$\langle \hat{H}_V \rangle = -\frac{N_s}{8} z_{\text{eff}} V_1 (n_{LB} - n_{SB})^2. \quad (5)$$

It vanishes again in the UN state, and provides an energy gain $-V_1 z_{\text{eff}} N_s/2$ in the FD state. Hence, the energy difference between the FD state and the uniform one reads, in the atomic limit:

$$\begin{aligned} E_{FD} - E_{UN} &= \frac{N_s}{2} [U^{\sigma\sigma} - z_{\text{eff}} V_1 - \Delta_s] \\ &= \frac{N_s}{2} [U - 3J - z_{\text{eff}} V_1 - \Delta_s] \end{aligned} \quad (6)$$

The transition into the charge-disproportionated state in the atomic limit occurs, therefore, when

$$U^{\sigma\sigma} - z_{\text{eff}} V_1 < \Delta_s. \quad (7)$$

Note that, if only the nearest-neighbor component of the non-local interactions is taken into account, the FD state is stable for $U^{\sigma\sigma} - zV_1 < \Delta_s$. The above criterion in the presence of long-range interaction simply amounts to replacing the connectivity of the lattice z by the effective Madelung connectivity.

Let us consider the orthorhombic phase where $\Delta_s = 0$. The above criterion then reads $U - 3J - z_{\text{eff}} V_1 < 0$. Hence, a small enough value of U (e.g. strongly reduced by screening) or a large enough value of the Hund's coupling J leads to an instability into the disproportionated state, as noted in previous work^{13,14}. In the present context, this instability is a spontaneous symmetry breaking of electronic origin, since there is only one type of sites in this crystal structure. Our cRPA results for LuNiO_3 in the orthorhombic phase yield $U^{\sigma\sigma} - z_{\text{eff}} V_1 \simeq -0.1 \text{ eV}$: the combined effect of screening and long-range interactions yields a small but negative value of this quantity, which is consistent with the physical picture of Subedi et al.¹³. Hence, in the atomic limit, we would conclude that the orthorhombic phase is spontaneously unstable to disproportionation! In reality, as shown below, the inclusion of inter-site hopping in a full DFT+DMFT treatment leads to the correct conclusion that the orthorhombic phase is not electronically disproportionated - the atomic-limit estimate providing a considerable overestimation of the range of stability of the FD state. However, inaccurate as it may

be (especially in the metallic state), the virtue of this atomic limit estimate is to emphasize how screening, a large J , and sizeable inter-site interactions can lead to disproportionation.

In the monoclinic phase, we obtained $U^{\sigma\sigma} = 0.74 \text{ eV}$, $V_1 = 0.44 \text{ eV}$, hence $U^{\sigma\sigma} - z_{\text{eff}} V_1 \simeq -0.03 \text{ eV}$. Basically any positive value of the Peierls energy gap, which is non-zero in this phase, will thus stabilize a fully disproportionated state in the atomic limit. As shown below, monoclinic LuNiO_3 is indeed found to be a disproportionated insulator when performing DFT+DMFT calculations with these interaction parameters.

D. DMFT: setup and double counting

We now turn to the results obtained in the DFT+DMFT framework, providing first some technical details about the calculation.

The one-electron part of the effective Hamiltonian is $\hat{H}_0 = \hat{H}_{\text{DFT}}^0 - \hat{H}_{dc}$. The DFT Hamiltonian was obtained using the FLAPW method as implemented in the Wien2k software package⁵⁰, with Perdew-Burke-Erzenhof (PBE) approximation⁵¹ for the exchange-correlation functional. A k-mesh of $6 \times 5 \times 4$ points is used. Projected local orbitals⁵² spanning the low-energy e_g subspace are constructed using the implementation of the TRIQS/DFTTOOLS software package⁵³⁻⁵⁶.

The full local self-energy arises from both the DMFT treatment of the local interactions H_U in (1) at the dynamical level and from the non-local interactions treated within the Hartree approximation, namely:

$$\Sigma_\alpha(i\omega_n) = \Sigma_\alpha^{\text{imp}}(i\omega_n) - \Sigma_{dc,\alpha}^{\text{imp}} + \Sigma_\alpha^V - \Sigma_{dc,\alpha}^V. \quad (8)$$

In this expression, $\alpha = \text{LB, SB}$ is an index labelling LB and SB sites, Σ_α^V is the Hartree self-energy:

$$\Sigma_\alpha^V = z_{\text{eff}} V_1 (n_{\bar{\alpha}} - n_\alpha)/2, \quad (9)$$

and $\Sigma_\alpha^{\text{imp}}(i\omega_n)$ is obtained by solving the DMFT effective impurity model using the hybridization-expansion continuous-time quantum Monte Carlo (CTQMC) algorithm TRIQS/CTHYB⁵⁵⁻⁵⁷.

A double counting (DC) correction must be included, in order to remove the contribution from interactions already included within DFT. This DC correction can be viewed equivalently as the \hat{H}_{dc} part of \hat{H}_0 or as part of the self-energy. The DC correction to the self-energy arising from the U, J interactions is evaluated in the fully-localized limit⁵⁸ as follows⁵³:

$$\Sigma_{dc,\alpha}^{\text{imp}} = \bar{U}(n_\alpha^{\text{DFT}} - 1/2) - \bar{J}(n_\alpha^{\text{DFT}}/2 - 1/2), \quad (10)$$

while the DC correction to the Hartree self-energy associated with the long-range interactions reads:

$$\Sigma_{dc,\alpha}^V = z_{\text{eff}} V_1 (n_{\bar{\alpha}}^{\text{DFT}} - n_\alpha^{\text{DFT}})/2. \quad (11)$$

In these expressions, $\bar{U} = U - J$ is the average interaction between electrons with opposite spins, $\bar{J} = \bar{U} - U^{\sigma\sigma} = 2J$,

and n_α^{DFT} is the occupancy of Ni e_g shell in DFT for the site $\alpha = \text{LB or SB}$.

In the monoclinic phase the two inequivalent Ni sites have different e_g occupancy already at the DFT level: $n_\alpha^{\text{DFT}} = 1.17$ and 0.83 for the LB and SB site, respectively. From the expressions above, one sees that the Peierls energy splitting between LB and SB sites appearing in $\hat{H}_0 = \hat{H}_{\text{DFT}}^0 - \hat{H}_{dc}$ is renormalized by double counting, as compared to its DFT value:

$$\Delta_s = \Delta_s^{\text{DFT}} + (U - 2J - z_{\text{eff}}V_1) \Delta n^{\text{DFT}}, \quad (12)$$

with $\Delta n^{\text{DFT}} = n_{\text{LB}}^{\text{DFT}} - n_{\text{SB}}^{\text{DFT}}$. Note that given the cRPA values above, $U - 2J - z_{\text{eff}}V_1 \simeq 0.32$ eV is positive so that double-counting enhances the effective value of the Peierls energy, from $\simeq 0.25$ eV at the DFT level to $\Delta_s \simeq 0.36$ eV.

E. DMFT: results and phase diagram

In order to explore how the values of the interaction strengths affect the physics of LuNiO_3 in each crystal structure, we have performed a series of DFT+DMFT calculations for a fixed value of $V_1 = 0.44$ eV with varying U and J . The obtained phase diagrams are presented in Fig. 4. The main qualitative features are similar to the results of Ref.13, in which the non-local interactions were not taken into account and only the local Kanamori interactions were included. Specifically, both the monoclinic and orthorhombic structures have a phase boundary separating a uniform metallic and a disproportionated (insulating or metallic) phase.

We note that the location of this boundary is very different for the orthorhombic and for the monoclinic phase, being pushed towards much smaller values of J for the latter. This demonstrates the strong sensitivity of the disproportionation to the value of the Peierls energy¹³.

The physical range of interaction parameters must be associated with regions of the phase diagram corresponding to the monoclinic phase being insulating and the orthorhombic one being metallic with uniform distribution of site occupancies (non-disproportionated metal). Because of the great sensitivity of the critical boundary to Δ_s , rather extended regions of the (U, J) parameter space satisfy these conditions (basically corresponding to the area delimited by the orthorhombic (blue) boundary to the right and the monoclinic (red) one to the left, including the range $J = 0.3 - 0.7$ and $U = 1.5 - 2.0$).

The calculated cRPA values are marked by a (yellow) diamond symbol on each panel of Fig. 4. They are located well within the metallic domain for the orthorhombic phase and just inside the insulating domain (rather close to the MIT boundary) for the monoclinic phase. These results demonstrate that cRPA is able to provide reasonable values of the effective screened interactions, which correctly account for the physical nature of each phase.

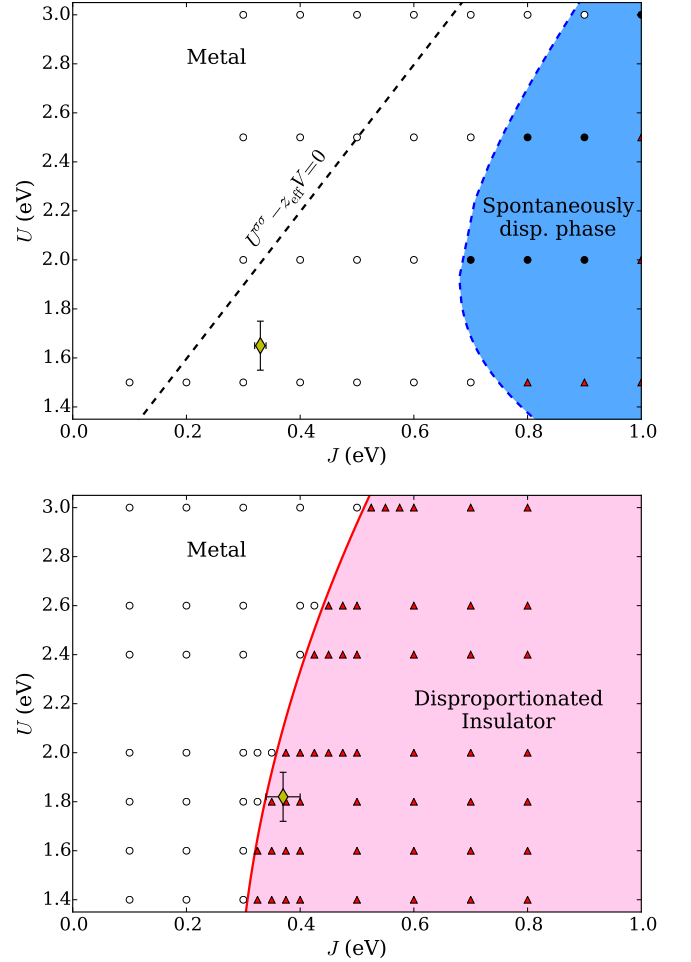


FIG. 4. Phase diagrams of the monoclinic (bottom) and orthorhombic (top) phases of LuNiO_3 . For the monoclinic phase: empty circles show metallic solutions, red triangles correspond to a disproportionated insulator. For the orthorhombic phase: empty circles stand for uniform metallic, filled circles – for disproportionated metallic, and red triangles – for disproportionated insulating solutions; the blue domain contains spontaneously disproportionated (metallic or insulating) solutions. The value of V_1 is fixed to the average cRPA value. The cRPA values of U and J are marked by the diamond, with error bars showing variations for different sites and orbitals.

V. DISCUSSION AND CONCLUSIONS

In summary, the question we have addressed in this article is that of the appropriate values of interaction parameters for rare-earth nickelates, when adopting a low-energy description of their electronic structure involving only the partially occupied e_g states. We have calculated these effective low-energy interaction parameters from first principles for LuNiO_3 , using the constrained random-phase approximation (cRPA). The obtained values confirm the strong reduction of the effective on-site U by screening, down to $U \simeq 1.65$ eV in the orthorhombic phase ($U \simeq 1.83$ eV in the monoclinic phase), while the Hund's coupling J remains sizeable ($J \simeq 0.33, 0.37$ eV in each phase, respectively).

The cRPA results also reveal the importance of the long-range intersite interactions, with a slow spatial decay V_1/R . V_1 is found to be of order $0.42 - 0.44$ eV so that these interactions must be included in a proper low-energy treatment. When treated at the level of a Hartree approximation, they lead to a further reduction of the effective parallel-spin local interaction $U_{\text{eff}}^{\sigma\sigma} = U - 3J - z_{\text{eff}}V_1$ (with z_{eff} the effective Madelung connectivity), which is found to be small and negative. This is qualitatively consistent with the picture of a negative charge-transfer insulator and validates the low-energy description advocated in earlier work^{13,14}. Let us also note that the low-energy interaction is further renormalized by higher-order many-body effects not taken into account in the present work, as well as by dynamical screening due to phonon modes. A rough estimate of the latter effect in nickelates suggests that it is small, but a more detailed study is left for future work. We have constructed an appropriate low-energy model based on the cRPA effective interactions, and solved this model in the DFT+DMFT framework. We found that the monoclinic structure falls within the bond-disproportionated-insulator region, while the orthorhombic structure is located deep in the uniform metallic state, in agreement with experimental observations. While our calculations take into account only electronic degrees of freedom, a full theory of the metal-insulator transition in nickelates should also take into account the coupling to the relevant lattice mode associated with the structural transition: this should be addressed in future work.

Besides the specific example of nickelates, our work can be put in the broader context of compounds with small or negative charge transfer leading to the possible formation of ligand holes. We have shown that it is possible to build an appropriate low-energy effective theory of such compounds, involving only electronic states near the Fermi level, provided

the strong reduction of the low-energy effective interactions is properly taken into account. This provides a perspective on these materials which is complementary to the one in which ligand states are explicitly retained in the description⁵⁻⁷. Future work should document the general applicability of the present approach by considering other compounds with small or negative charge transfer.

ACKNOWLEDGMENTS

We are grateful to Manuel Bibes, Sara Catalano, Claude Ederer, Marta Gibert, Alexander Hampel, Marisa Medarde, Andrew J. Millis, Yusuke Nomura, Swarup Panda, Julien Ruppen, George Sawatzky, Hugo Strand, Alaska Subedi, Jean-Marie Tarascon, Jérémie Teyssier, Jean-Marc Triscone, Dirk van der Marel, and Julien Varignon for numerous discussions about the physics of rare-earth nickelates. This work was supported by the European Research Council grants ERC-319286-‘QMAC’ (A.Georges), ERC-278472-‘MottMetals’ (O.Parcollet, P. S.), ERC-617196-‘CorrelMat’ (S.Biermann, P. S.) and IDRIS/GENCI Orsay under project 201601393. L. Pourovskii acknowledges computational resources provided by the Swedish National Infrastructure for Computing (SNIC) at the National Supercomputer Centre (NSC) and PDC Center for High Performance Computing. O. Peil and A. G. acknowledge support from the Swiss National Science Foundation NCCR MARVEL and computing resources provided by the Swiss National Supercomputing Centre (CSCS) under projects s575 and mr17. M. B. gratefully acknowledges financial support from the Helmholtz Association through the Helmholtz Postdoctoral Programme (VH-PD-022). F. A. acknowledges financial support from the Swedish Research Council (VR).

-
- ¹ M. Imada, A. Fujimori, and Y. Tokura, *Rev. Mod. Phys.* **70**, 1039 (1998).
 - ² F. Zhang and T. Rice, *Phys. Rev. B* **37**, 7 (1988).
 - ³ J. Zaanen, G. Sawatzky, and J. Allen, *Phys. Rev. Lett.* **55**, 418 (1985).
 - ⁴ J. Varignon, M. N. Grisolia, J. Iñiguez, A. Barthélémy, and M. Bibes, *ArXiv e-prints* (2016), arXiv:1603.05480 [cond-mat.mtrl-sci].
 - ⁵ T. Mizokawa, H. Namatame, A. Fujimori, K. Akeyama, H. Kondo, H. Kuroda, and N. Kosugi, *Phys. Rev. Lett.* **67**, 1638 (1991).
 - ⁶ T. Mizokawa, A. Fujimori, H. Namatame, K. Akeyama, and N. Kosugi, *Phys. Rev. B* **49**, 7193 (1994).
 - ⁷ T. Mizokawa, D. I. Khomskii, and G. A. Sawatzky, *Phys. Rev. B* **61**, 11263 (2000).
 - ⁸ S. Johnston, A. Mukherjee, I. Elfimov, M. Berciu, and G. A. Sawatzky, *Phys. Rev. Lett.* **112**, 106404 (2014).
 - ⁹ H. U. R. Strand, *Phys. Rev. B* **90**, 155108 (2014).
 - ¹⁰ A. Demourgues, F. Weill, B. Darriet, A. Wattiaux, J. Grenier, P. Gravier, and M. Pouchard, *Journal of Solid State Chemistry* **106**, 330 (1993).
 - ¹¹ V. Bisogni, S. Catalano, R. J. Green, M. Gibert, R. Scherwitzl, Y. Huang, V. N. Strocov, P. Zubko, S. Balandeh, J.-M. Triscone, G. Sawatzky, and T. Schmitt, *Nature Comm.* **7**, 13017 (2016).
 - ¹² H. Park, A. J. Millis, and C. A. Marianetti, *Phys. Rev. Lett.* **109**, 156402 (2012).
 - ¹³ A. Subedi, O. E. Peil, and A. Georges, *Phys. Rev. B* **91**, 075128 (2015).
 - ¹⁴ I. I. Mazin, D. I. Khomskii, R. Lengsdorf, J. A. Alonso, W. G. Marshall, R. M. Ibberson, A. Podlesnyak, M. J. Martínez-Lope, and M. M. Abd-Elmeguid, *Phys. Rev. Lett.* **98**, 176406 (2007).
 - ¹⁵ A. Georges, G. Kotliar, W. Krauth, and M. J. Rozenberg, *Rev. Mod. Phys.* **68**, 13 (1996).
 - ¹⁶ J. Ruppen, J. Teyssier, O. E. Peil, S. Catalano, M. Gibert, J. Mravlje, J.-M. Triscone, A. Georges, and D. van der Marel, *arXiv:1509.09245 [cond-mat]* (2015), arXiv: 1509.09245.
 - ¹⁷ J. Ruppen, J. Teyssier, I. Ardiszone, O. E. Peil, S. Catalano, M. Gibert, J. M. Triscone, A. Georges, and D. van der Marel, *ArXiv e-prints* (2017), arXiv:1702.00601 [cond-mat.str-el].
 - ¹⁸ F. Aryasetiawan, M. Imada, A. Georges, G. Kotliar, S. Biermann, and A. I. Lichtenstein, *Phys. Rev. B* **70**, 195104 (2004).
 - ¹⁹ T. Miyake and F. Aryasetiawan, *Phys. Rev. B* **77**, 085122 (2008).
 - ²⁰ L. Vaugier, H. Jiang, and S. Biermann, *Phys. Rev. B* **86**, 165105 (2012).
 - ²¹ B.-C. Shih, Y. Zhang, W. Zhang, and P. Zhang, *Phys. Rev. B* **85**,

- 045132 (2012).
- ²² B. Amadon, T. Applencourt, and F. Bruneval, Phys. Rev. B **89**, 125110 (2014).
 - ²³ A. van Roekeghem, L. Vaugier, H. Jiang, and S. Biermann, Phys. Rev. B **94**, 125147 (2016).
 - ²⁴ S. K. Panda, H. Jiang, and S. Biermann, “Pressure dependence of dynamically screened coulomb interactions in nio: Effective hubbard, hund, intershell, and intersite components,” 2017.
 - ²⁵ P. Seth, P. Hansmann, A. van Roekeghem, L. Vaugier, and S. Biermann, “Towards a first-principles determination of effective coulomb interactions in correlated materials: Role of inter-shell interactions,” 2017.
 - ²⁶ J. A. Alonso, M. J. Martínez-Lope, M. T. Casais, J. L. García-Muñoz, and M. T. Fernández-Díaz, Phys. Rev. B **61**, 1756 (2000).
 - ²⁷ C. Friedrich, S. Blügel, and A. Schindlmayr, Phys. Rev. B **81**, 125102 (2010).
 - ²⁸ S. Blügel and G. Bihlmayer, in *Computational Nanoscience: Do It Yourself! NIC Series Vol. 31*, edited by J. Grotendorst, S. Blügel, and D. Marx (John von Neumann Institute for Computing, Jülich, 2006) p. 85, <http://www.flapw.de>.
 - ²⁹ A. A. Mostofi, J. R. Yates, Y.-S. Lee, I. Souza, D. Vanderbilt, and N. Marzari, Comp. Phys. Commun. **178**, 685 (2008).
 - ³⁰ P. Hansmann, L. Vaugier, H. Jiang, and S. Biermann, Journal of Physics: Condensed Matter **25**, 094005 (2013).
 - ³¹ P. Hansmann, T. Ayrál, L. Vaugier, P. Werner, and S. Biermann, Phys. Rev. Lett. **110**, 166401 (2013).
 - ³² P. Hansmann, T. Ayrál, A. Tejada, and S. Biermann, Scientific Reports **6**, 19728 (2016).
 - ³³ T. Miyake, F. Aryasetiawan, and M. Imada, Phys. Rev. B **80**, 155134 (2009).
 - ³⁴ E. Şaşıoğlu, C. Friedrich, and S. Blügel, Phys. Rev. B **83**, 121101 (2011).
 - ³⁵ We mention in passing that we have developed an application of the TRIQS/DFTTOOLS package^{37,53–56} which provides an interface to the FLEUR electronic structure code.
 - ³⁶ C. Friedrich, A. Schindlmayr, S. Blügel, and T. Kotani, Phys. Rev. B **74**, 045104 (2006).
 - ³⁷ G. Michalíček, M. Betzinger, C. Friedrich, and S. Blügel, Computer Physics Communications **184**, 2670 (2013).
 - ³⁸ M. Schüler, M. Rösner, T. O. Wehling, A. I. Lichtenstein, and M. I. Katsnelson, Phys. Rev. Lett. **111**, 036601 (2013).
 - ³⁹ J. Merino and R. H. McKenzie, Phys. Rev. Lett. **87**, 237002 (2001).
 - ⁴⁰ A. Amaricci, A. Camjayi, K. Haule, G. Kotliar, D. Tanasković, and V. Dobrosavljević, Phys. Rev. B **82**, 155102 (2010).
 - ⁴¹ T. Ayrál, P. Werner, and S. Biermann, Phys. Rev. Lett. **109**, 226401 (2012).
 - ⁴² T. Ayrál, S. Biermann, and P. Werner, Phys. Rev. B **87**, 125149 (2013).
 - ⁴³ L. Huang, T. Ayrál, S. Biermann, and P. Werner, Phys. Rev. B **90**, 195114 (2014).
 - ⁴⁴ T. Yoshida and C. Hotta, Phys. Rev. B **90**, 245115 (2014).
 - ⁴⁵ E. G. C. P. van Loon, M. I. Katsnelson, and M. Lemieshko, Phys. Rev. B **92**, 081106 (2015).
 - ⁴⁶ T. Ayrál, S. Biermann, and P. Werner, Phys. Rev. B **94**, 239906 (2016).
 - ⁴⁷ E. G. C. P. van Loon, M. Schüler, M. I. Katsnelson, and T. O. Wehling, Phys. Rev. B **94**, 165141 (2016).
 - ⁴⁸ T. Ayrál, S. Biermann, P. Werner, and L. Boehnke, Phys. Rev. B **95**, 245130 (2017).
 - ⁴⁹ H. Terletska, T. Chen, and E. Gull, Phys. Rev. B **95**, 115149 (2017).
 - ⁵⁰ P. Blaha, K. Schwarz, G. K. H. Madsen, D. Kvasnicka, and J. Luitz, *WIEN2K, An Augmented Plane Wave + Local Orbitals Program for Calculating Crystal Properties* (Karlheinz Schwarz, Techn. Universität Wien, Austria, 2001).
 - ⁵¹ J. P. Perdew, K. Burke, and M. Ernzerhof, Phys. Rev. Lett. **77**, 3865 (1996).
 - ⁵² B. Amadon, F. Lechermann, A. Georges, F. Jollet, T. Wehling, and A. Lichtenstein, Phys. Rev. B **77**, 205112 (2008).
 - ⁵³ M. Aichhorn, L. Pourovskii, V. Vildosola, M. Ferrero, O. Parcollet, T. Miyake, A. Georges, and S. Biermann, Phys. Rev. B **80**, 085101 (2009).
 - ⁵⁴ M. Aichhorn, L. Pourovskii, P. Seth, V. Vildosola, M. Zingl, O. E. Peil, X. Deng, J. Mravlje, G. J. Kraberger, C. Martins, M. Ferrero, and O. Parcollet, Comp. Phys. Commun. **204**, 200 (2016).
 - ⁵⁵ O. Parcollet, M. Ferrero, T. Ayrál, H. Hafermann, I. Krivenko, L. Messio, and P. Seth, Comp. Phys. Commun. **196**, 398 (2015).
 - ⁵⁶ TRIQS: a Toolbox for Research on Interacting Quantum Systems, <http://ipht.cea.fr/triqs>.
 - ⁵⁷ P. Seth, I. Krivenko, M. Ferrero, and O. Parcollet, Comp. Phys. Commun. **200**, 274 (2016).
 - ⁵⁸ V. I. Anisimov, F. Aryasetiawan, and A. I. Lichtenstein, Journal of Physics: Condensed Matter **9**, 767 (1997).